

Targeting Studies for a Second-Generation Mu2e Experiment

Takumi Matsuzawa¹, Thomas J. Roberts², Eric Prebys³

¹*Kalamazoo College, Kalamazoo, Michigan 49006, USA*

²*Muons, Inc., Batavia, Illinois 60510, USA*

³*Fermi National Accelerator Laboratory, Batavia, Illinois 60510, USA*

(Dated: August 17, 2015)

The target of a next-generation Mu2e experiment (Mu2e-II) is to achieve a sensitivity approximately by a factor ten better than the currently planned Mu2e facility. An 800 MeV proton beam with high intensity will be available after the completion of the Proton Improvement Plan-II. We investigated the potential of using the beam for Mu2e-II using G4beamline. The number of stopped muons at the stopping target per kilowatt dropped by a factor of 1.633, indicating Mu2e-II will produce 7.653 times more stopped muons than Mu2e during 3 years with 10 times the power available from PIP-II. The proton beam can be delivered to the production target by modifying the magnets of the beam transport. We optimize the beam trajectory and position of the production target, and determined the muon stopping rate for Mu2e-II with the optimized orientation.

I. INTRODUCTION

The Mu2e experiment will search for a charged-lepton-flavor violation process of coherent muon-to-electron conversion in the presence of nucleus with a sensitivity of four orders of magnitude beyond the current limit. The current experimental limit is 7×10^{-13} (90% C.L.) from the SINDRUM-II experiment [1]. A second-generation Mu2e experiment (Mu2e-II) targets to achieve approximately ten times better sensitivity than Mu2e. The factor of ten was chosen because this plan should be achievable by only modest changes to the facilities of the Mu2e experiment.

A. Charged-Lepton-Flavor Violation

The muon-to-electron conversion process is an example of charged-lepton-flavor violation (CLFV). Lepton numbers in each generation were strictly conserved in the Standard Model for any interaction until neutrinos were discovered to have mass. In a simple extension of the Standard Model that includes neutrino oscillations, the rate of the muon-to-electron conversion is far lower than the experimental limit; however, several theories beyond the Standard Model predict CLFV with a higher rate. Hence, an observation of CLFV is a signal of new physics.

Experiments using muons to search for CLFV were constructed by three processes: $\mu \rightarrow e\gamma$, $\mu^+ \rightarrow e^+e^-e^+$, and the coherent $\mu^-N \rightarrow e^-N$ conversion process in nuclei. Limits for branch ratios (Br) are set for $\mu \rightarrow e\gamma$, and $\mu^+ \rightarrow e^+e^-e^+$ processes. The rate for the coherent $\mu^-N \rightarrow e^-N$ conversion process in nuclei is measured by,

$$R_{\mu e} = \frac{\Gamma(\mu^-N(A, Z) \rightarrow e^-N(A, Z))}{\Gamma(\mu^-N(A, Z) \rightarrow \nu_\mu N(A, Z-1))}, \quad (1)$$

where $N(A, Z)$ denotes a nucleus with mass number A and atomic number Z . The numerator corresponds to

the rate for the CLFV conversion process and the denominator corresponds to the rate for ordinary muon capture on the same nucleus. The current experimental limits are following: $Br(\mu^+ \rightarrow e^+\gamma) < 5.7 \times 10^{-13}$ [2], $Br(\mu^+ \rightarrow e^+e^-e^+) < 1 \times 10^{-12}$ [3], $R_{\mu e} < 7 \times 10^{-13}$ [4]. The target sensitivity of the Mu2e experiment is $R_{\mu e} < 2.87 \times 10^{-17}$ [1], which is an improvement by about 4 orders of magnitude.

B. Mu2e Experiment and Upgrade

The concept of the Mu2e experiment is to stop muons in thin aluminum foils to form muonic atoms, and then measures the resulting electron spectrum. The signal would produce mono-energetic electrons with energy of 105 MeV. Besides this rare conversion, about 40% of the stopped muons decay in orbit, producing electrons, muon neutrinos, and anti-electron neutrinos. About 60% of the stopped muons are captured on nucleus.

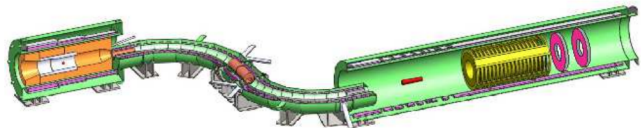


FIG. 1. The experimental Setup for Mu2e. The pulsed proton beam enters to the production solenoid (far left) from the top right. Produced pions and muons travel the S-shaped Transport Solenoid (TS). Most of pions decay into muons during TS. Muons with low momentum enter the Detector Solenoid (right). Muons are stopped at the aluminum target (red). Electrons produced in the stopping target are then transported through the trackers, where the momentum is measured. The electrons strikes the calorimeters, where the energy is independently measured.

The upgrade for the Mu2e experiment is planned to achieve approximately 10 times better sensitivity. Regardless the result of Mu2e, Mu2e-II will be interesting.

If Mu2e observes completely consistent with background, Mu2e-II should further investigate the parameter space beyond the standard model. If Mu2e observes a 3σ excess, 10 times better sensitivity will definitely resolve the situation. If Mu2e observes CLFV, Mu2e-II could explore different stopping targets such as titanium and gold to untangle the underlying physics. Mu2e-II will be possible by the proposed Proton Improvement Plan-II (PIP-II) at Fermilab which is an upgrade of its proton accelerator complex based on the construction of a superconducting radio frequency linac. After the completion of PIP-II, an 800 MeV proton beam will be available. Beam power is expected to increase from current 8 kW to 100 kW.

Here, we explore advantages and disadvantages of the currently planned upgrade of the Mu2e experiment. Properties of the beamlines for Mu2e and Mu2e-II are summarized in Table I. Our goal is to investigate the muon stopping rate for both cases. We then explore possibility of targeting the proton beam to the production target by only modest changes to the Mu2e design.

TABLE I. Beamline assumption.

	Mu2e	Mu2e-II
Beam Kinetic Energy	8 GeV	800 MeV
Beam Power	8 kW	8-100 kW
Protons-On-Target (POT)	3.6×10^{20}	$3.6 \times 10^{21} - 4.5 \times 10^{22}$
Run Duration	3 years	3 years
Run Time	2×10^7 sec/year	2×10^7 sec/year
Duty Factor	0.32	0.90
POT Pulse Full Width	200 ns	-
POT Pulse Spacing	1695 ns	-
POT Extinction	$<1 \times 10^{-10}$	$<1 \times 10^{-12}$ *

*expected

II. SIMULATION

We use G4Beamline v2_16 as developed at Muons, Inc., which is a particle tracking simulation program based on Geant4. Our simulations are based on Mu2e.in in the Mu2e CVS repository. In all instances we simulate with the full Mu2e solenoid system including all collimators, the production solenoid, transport solenoid, detector solenoid, and the latest magnetic-field map. Parameters for both scenarios are described in Table II. To determine the muon stopping rate, we set the starting position of the beam 2 mm in front of the production target. The timing distribution of the proton beam can be modeled as a delta function.

To explore ways to transport the 800 MeV proton beam to the production target, we first scale the field strength of the trim magnets by momentum, and then optimize the field strength of the vertical trim magnet, located closest to the holes in the transport solenoid, so that the proton beam can enter the production solenoid with minimal loss. After the optimization of the trim

TABLE II. Proton beam parameters considered in this study. The assumed proton mass is 938.272 MeV.

	Kinetic Energy	Momentum	Simulated Events
Mu2e	8 GeV	8.889 GeV/c	40×10^6
Mu2e-II	800 MeV	1.463 GeV/c	300×10^6

magnet, trajectory of the 800 MeV is used to configure the position of the production target. Finally, we study the muon stopping rate for Mu2e-II with the optimized condition.

III. RESULTS AND DISCUSSION

A. Muon Stopping Rate

The muon stopping rates for Mu2e and Mu2e-II are determined as presented in Table III. The result shows that a couple of muons are stopped per 1000 protons for Mu2e. This is consistent with the previous study [5]. The number of stopped muons per POT for Mu2e-II drops by a factor of 16.3. In terms of power, the stopping rate for Mu2e-II drops by a factor of 1.63. Assuming that Mu2e-II runs with beam power of 100 kW from the beginning, it would produce 4.657×10^{18} stopped muons. This is 7.65 times more stopped muons than Mu2e.

TABLE III. Muon stopping rate.

Kinetic Energy	Stops / POT	Stops / kW
8 GeV	1.690×10^{-3}	7.607×10^{16}
800 MeV	1.035×10^{-4}	4.657×10^{16}

It is uncertain why the muon stopping rate drops by only a factor of 1.63. Figure 2 and 3 show the momentum distribution of muons before and after the transport solenoid. As protons hit the production target, pions and muons are produced. The momentum distribution of muons for Mu2e have a longer tail than Mu2e-II due to the higher proton beam energy. A longer tail is also observed with the momentum distribution of pions for Mu2e. The transport solenoid selects only muons with low momentum between 15 and 100 MeV/c. As shown in Fig. 2 and 3, the momentum distributions of muons after the transport solenoid for Mu2e and Mu2e-II looks very alike. This indicates following. Because Mu2e produces muons with broader momentum distribution, the fraction of muons that survive the transport solenoid is smaller than Mu2e-II.

After muons pass through the transport solenoid, 37.6% of them are stopped at the aluminum target for Mu2e. Similarly, 38.0% of muons are stopped for Mu2e-II. This can be also explained by the momentum distribution of muons after the transport solenoid.

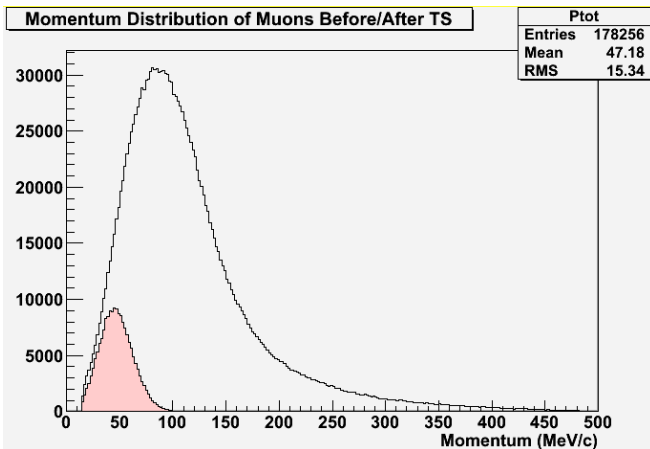


FIG. 2. Momentum distribution of muons before (black) and after (red) the transport solenoid (Mu2e). Only muons with low momentum pass the transport solenoid.

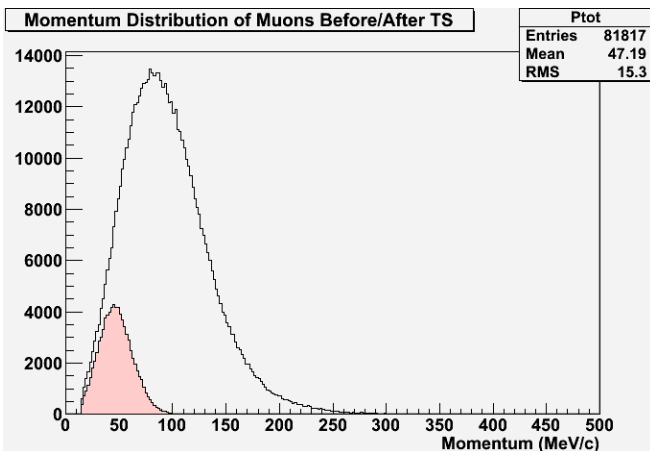


FIG. 3. Momentum distribution of muons before (black) and after (red) the transport solenoid (Mu2e-II). Only muons with low momentum pass the transport solenoid.

B. Arrival Time of Muons

The arrival time of muons is important to consider the timing structure of the proton beam for Mu2e-II. Because of PIP-II, Mu2e-II will not be constrained to the timing structure of Mu2e. As shown in Figure 4 and 5, the arrival time of muons to the stopping target is independent of proton beam energy. This result is explained because the momentum distribution of muons after the transport solenoid looks alike between Mu2e and Mu2e-II. The proton timing structure can be tuned to reduce the background and increase the muon acceptance as much as possible. As the arrival time of muons and pions for Mu2e-II will be very similar to the arrival time of Mu2e, we can wait until the prompt background such as radiative pion capture occurs. Because the proton pulse width is expected to be narrower for Mu2e-II, we can also lengthen the live gate.

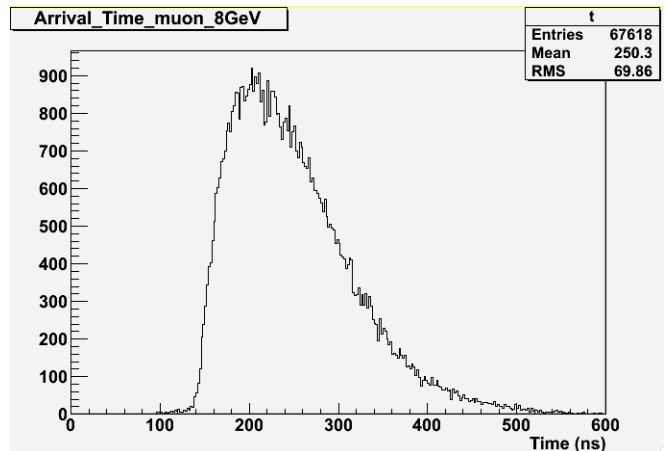


FIG. 4. Arrival time of muons for Mu2e. Protons hit the production target at $t=0$.

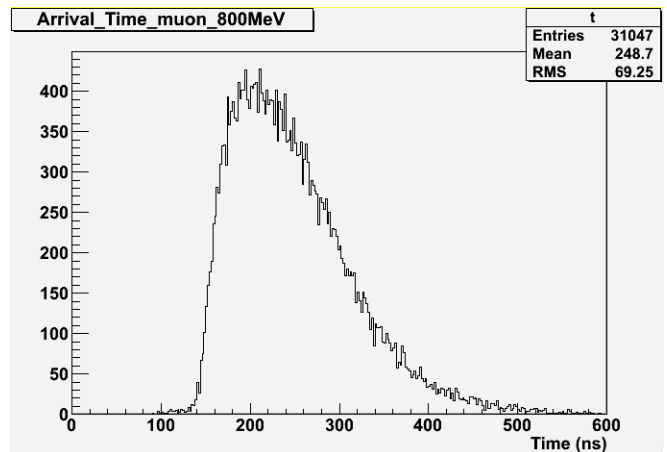


FIG. 5. Arrival time of muons for Mu2e-II. Protons hit the production target at $t=0$.

C. Targeting Study for Mu2e-II

Some modifications to the current design must be made to use the 800 MeV pulsed proton beam instead of 8 GeV beam of Mu2e. We first scale down the field strength of the magnets in the beam transport system by the ratio of proton momentum. We optimize its trajectory by minimizing the sum of distances between the center of holes and the beam. This is done by changing the field strength of only the last vertical trim magnet.

As clearly shown in Fig. 6, the 800 MeV beam does not hit the production target as it is set for the 8 GeV beam. To get protons to the target, there are two possibilities. It is either moving the production target or making the holes in the transport solenoid bigger as well as modifying the beam transport system. In this study, we move the production target along the optimized trajectory of protons.

First, the trajectory of the 800 MeV beam is optimized to pass the holes in the transport solenoid. The beam

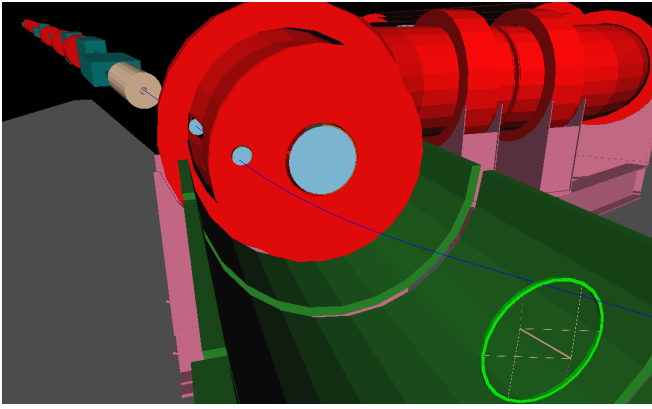


FIG. 6. An optimized trajectory of the 800 MeV proton beam is shown as a blue curve. The red object at the center is the transport solenoid. The production target is shown on the bottom right. Red and dark green objects on the top left are magnets of the beam transport system. The bright green ring indicates a size of the heat and radiation shield. The beam is transported through magnets, and passes through the holes in the transport solenoid, entering the production solenoid.

does not go through the centers of the holes when the magnets in the transport system are scaled down by a factor of the ratio of proton momentum. To optimize the trajectory, we add the displacement from each center, d_1 and d_2 , and minimize the sum. Figure 7 shows the displacement vs $\frac{1}{\rho}$ where ρ is the bending radius of the last vertical trim magnet. The inverse of ρ is proportional to the magnetic field strength by a relation, $B = \frac{p}{q\rho}$ where p is momentum, and q is the particle charge.

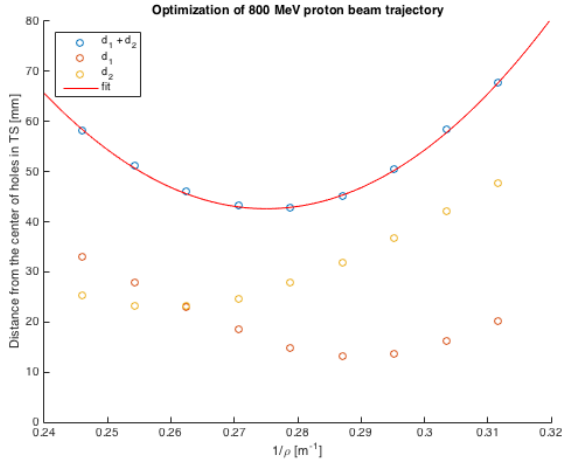


FIG. 7. The trajectory of the 800 MeV proton beam is optimized by minimizing the displacements from the center of each hole in the transport solenoid. Quadratic regression equation is $y = 18752x^2 - 10315x + 1461.1$.

Second, the position of the production target is modified so that the 800 MeV proton beam hits the target. A major constraint is the geometry of the production

solenoid because the radius of the cavity is only 200 mm (Fig. 8). As shown in Fig. 6, the proton beam hits the heat and radiation shield at the current position. The position of target is constrained inside the cavity.

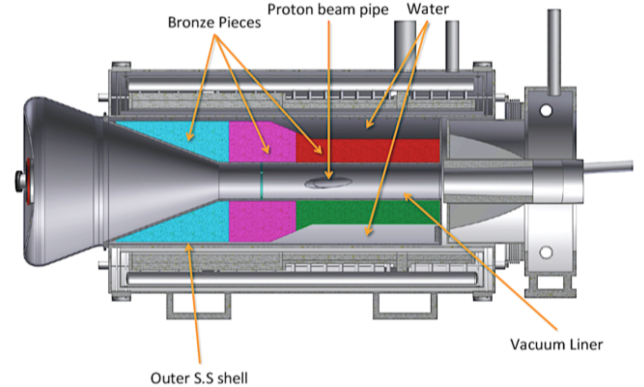


FIG. 8. The model of the production solenoid [1]. The radius of the cavity at the production target is 200 mm. Colored objects are heat and radiation shields.

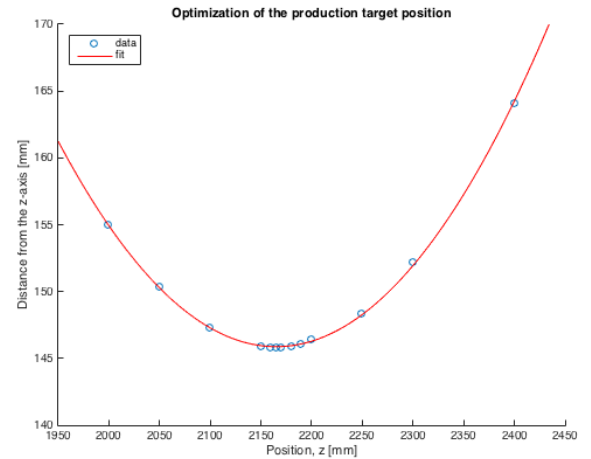


FIG. 9. The position of the production target is optimized by minimizing the distance from the z-axis. The z-axis goes through the center of the cavity. Distance between the proton beam trajectory and the z-axis is plotted. Quadratic regression equation is $y = 0.00033258x^2 - 1.44x + 1704.6$. Note that the target is positioned at $z=1764.5$ for Mu2e.

With an assumption that the proton beam travels along the optimized trajectory, we may optimize the position of the beam position by minimizing the displacement from the z-axis that goes through the center of the cavity. Figure 9 shows that the closest distance between the proton beam and the z-axis is approximately 145 mm. Considering the radius of the cavity, this could be problematic since it is too close to the shield. Particles may hit the shield as soon as they are produced. Note that the production target is positioned at $(x, y, z)=(0, 0, 1764.5)$ for Mu2e. The unit is in millimeter here. The coordinate

system follows as defined in the Mu2e.in from the Mu2e CVS repository. With this optimization for Mu2e-II, the production target is positioned at $(x, y, z)=(100.2, 106.0, 2164.7)$. It should be noted that the production target must be angled in a different way from the Mu2e design. Figure 10 shows the orientation of the production target along the optimized trajectory of the proton beam.

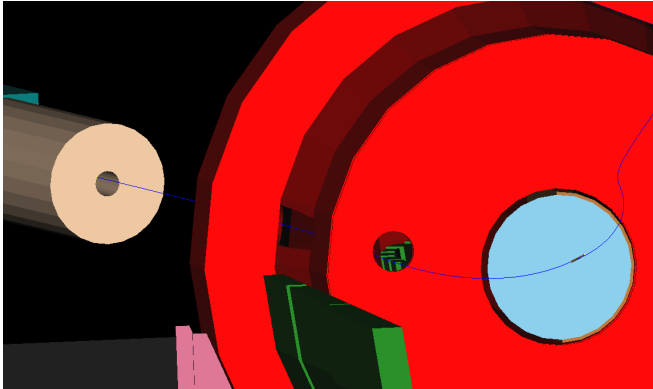


FIG. 10. The target was placed at the optimized position. The 800 MeV beam penetrates the target.

We explored the muon stopping rate for Mu2e-II with the optimized beam trajectory and the position of the production target as determined above. Note, however, that the proton beam after the target does not exit the production solenoid as in Mu2E, but rather hits the heat and radiation shield. This is probably not acceptable. The muon stopping rate was comparatively small since the target was positioned too far from the center of the transport solenoid.

IV. SUMMARY AND CONCLUSION

We investigated the stopping muon rate for the Mu2e and Mu2e-II experiment. Mu2e-II uses as much of the currently planned facilities, and the 800 MeV proton beam of PIP-II. We used G4beamline simulation to determine the muon stopping rate for Mu2e and Mu2e-II, and explored how to deliver the proton beam to the production target for Mu2e-II. The target sensitivity of Mu2e-II is 2.87×10^{-18} . With an assumption of running the experiment for 3 years with beam power of 100 kW, Mu2e-II would produce 4.657×10^{18} stopped muons which is 7.65 times more muons stopped of Mu2e with the same

run time. This proves that Mu2e-II has enough potential to achieve the target sensitivity. Additionally, the 800 MeV proton beam would eliminate the anti-proton-induced background. The proton timing structure can also be tuned to reduce backgrounds and increase muon acceptance as much as possible after PIP-II.

It is possible to deliver the 800 MeV proton beam into the production solenoid by scaling down the field strength of the magnets in the transport system; however, the production target must be located along the beam trajectory. With the current orientation, the production target must be positioned about 140 mm away from the z-axis even at the optimized position. The muon stopping rate for Mu2e-II with the performed optimization is not high because the target has to be positioned too far from the center of the transport solenoid.

The future work should explore muon yields when the production target is located at different positions along the beam trajectory. Also, we should seriously explore possibility of making the holes of the transport solenoid bigger. This method may allow positioning the production target along the z-axis. Preferably, the target should be positioned at $z=1000-2500$ mm to keep the muon yield high[6]. We must also explore methods of removing the proton beam after the target to dump it external to the production solenoid. Investigating the backgrounds and hadronic flash for Mu2e-II is also important. While the cosmic ray background seems to be under control for Mu2e, it must be considered for Mu2e-II since it has been a limiting factor in past experiments [7]. Investigation of veto rates must still be performed.

V. ACKNOWLEDGEMENTS

The project was carried out as a part of Lee Teng internship at Fermilab during the summer of 2015. I am very grateful to my mentor, Thomas J. Roberts for his valuable advice and continuous guidance, Eric Prebys and Tanja Waltrip for organizing the Lee Teng Undergraduate Internship. I would also like to thank Peter Kasper for his technical support with G4beamline. I also thank William A. Barletta, Linda Spentzouris, and Elvin R. Harms for teaching me accelerator physics at US Particle Accelerator School. Finally, I thank the Fermi National Accelerator Laboratory, and the Illinois Accelerator Institute for funding the project.

[1] Mu2e Collaboration, "Mu2e Technical Design Report," 2014.
 [2] J. Adam *et al.* (MEG Collaboration), arXiv:1303.0754.
 [3] U. Bellgardt *et al.* (SINDRUM Collaboration), Nucl. Phys. B **299**, 1 (1988).

[4] W. H. Bertl *et al.* (SINDRUM-II Collaboration), Eur. Phys. J. C **47**, 337 (2006).
 [5] K. Knoepfel *et al.* (Mu2e Collaboration), "Feasibility Study for a Next-Generation Mu2e Experiment," 2013, arXiv:1307.1168.

- [6] R. Coleman (Presentation), "Mu2e Experiments and Issues," 2012.
- [7] S. Ahmad, G. Azuelos, M. Blecher, D. A. Bryman, R. A. Burnham, E. T. H. Clifford, P. Depommier, M. S. Dixit *et al.*, Phys. Rev. D **38**, 2102 (1988).